do Amaral Camara Lima *et al. Carbon Footprints* 2023;2:20
DOI: 10.20517/cf.2023.08

Carbon Footprints

Original Article

Open Access

Check for updates

Carbon sequestration and geochronology in Southern England's seagrass meadows

Mariana do Amaral Camara Lima[1], Raymond D. Ward[2,3], Chris B. Joyce[3]

[1]School of Science, Engineering & Environment, University of Salford, Manchester M5 4WT, UK.
[2]Institute of Agriculture and Environmental Sciences, Estonian University of Life Sciences, Tartu 51014, Estonia.
[3]Centre for Aquatic Environments, School of Applied Sciences, University of Brighton, Brighton BN2 4GJ, UK.

Correspondence to: Dr. Mariana do Amaral Camara Lima, School of Science, Engineering & Environment, University of Salford, Manchester M5 4WT, UK. E-mail: M.doamaralcamaralima@salford.ac.uk

How to cite this article: do Amaral Camara Lima M, Ward RD, Joyce CB. Carbon sequestration and geochronology in Southern England's seagrass meadows. *Carbon Footprints* 2023;2:20. https://dx.doi.org/10.20517/cf.2023.08

Received: 26 Mar 2023 **First Decision:** 26 Jun 2023 **Revised:** 24 Jul 2023 **Accepted:** 25 Sep 2023 **Published:** 28 Sep 2023

Academic Editor: Daniel Alongi **Copy Editor:** Fangling Lan **Production Editor:** Fangling Lan

Abstract

The aim of this study was to provide an evaluation of the current methods used to assess carbon sequestration (C_{seq}) rates from intertidal *Zostera* spp. meadows in central Southern England. This study evaluated the use of ^{210}Pb dating methods to calculate sediment accretion rates from four intertidal seagrass meadows along the southern central coast of England. Results obtained were then used to determine C_{seq} rates, following different models. The mean rate of C_{seq} calculated in this study using the CRS model was 75.12 g m^{-2} $year^{-1}$, comparable to other global regions and within the estimated global range. However, results revealed that other, conservative methods, provide much lower C_{seq} rates, highlighting the need for caution when choosing appropriate methods and reporting results related to seagrass carbon sequestration potential. Moreover, these results highlight the importance of local assessments of C_{seq}, and the need to create robust models that include the effects of mixing, erosion, and disturbance, to better understand the possible effects of extreme climate events and anthropogenic impacts on seagrass ecosystems' carbon sequestration potential.

Keywords: Seagrass, blue carbon, carbon sequestration, sediment accretion, ^{210}Pb

INTRODUCTION

Vegetated coastal environments, including seagrass meadows, have been increasingly recognised for their ecosystem services associated with climate change mitigation, mainly related to their high primary

productivity and carbon sequestration potential[1-3]. Carbon sequestration (C_{seq}) is here described as the biophysical process in which plants capture and securely store atmospheric carbon dioxide (CO_2) as organic carbon (C_{org}) in their biomass and sediments[4]. Mean global C_{seq} rates in seagrass beds have been estimated as 220.7 g C m^{-2} $year^{-1}$, which translates to global sequestration rates of 35.31 × 10^{12} g C $year^{-1}$[5]. However, studies that successfully quantified C_{seq} rates from seagrass sediments reported high variability in results, mainly attributed to variations among habitats and species, and the low reliability of the long-term sediment accretion rates obtained from these environments[3,6-10]. Therefore, reputable estimations aimed at including seagrass meadows' C_{seq} and storage capacity in climate change and sea level rise mitigation strategies must be derived from multiple and site-specific sequestration rates, based on calculations that include pertinent pathways (burial and/or bicarbonate/if applicable), rather than simply using values from the literature[5,11-13].

Reliable measurements of sediment accretion rates should be used in conjunction with carbon density data to produce accurate estimates of C_{seq} rates for seagrass ecosystems[14]. Sediment accretion rates and elevation change in seagrasses meadows worldwide have thus far been determined by various methods, including mapping techniques (e.g., Altus altimeter, Stanley Compulevel, topographic surveys)[15,16], sediment traps[17] and alternatively, radionuclide dating methods using lead (^{210}Pb), carbon (^{14}C), as well as the artificial radionuclide Caesium (^{137}Cs), and other isotopes[18-21]. Sediment radionuclide dating provides estimates of sedimentation rates from decades to centuries and up to millennia and can then be coupled with the amount of C_{stock} per dated section, to assess carbon sequestration rates and provide long-term accretion data[14-22].

Out of the available radionuclide isotopes ^{210}Pb dating is the most widely utilised method for more recent (~150 years) sediment profiles, with a half-life of 22.26 years, providing a time frame compatible with recorded management actions and enabling the determination of fluctuations in carbon sequestration rates related to natural or human recorded timeframes[3,18,23,24]. Many low-energy marine ecosystems are associated with the steady build-up of autochthonous organic and inorganic material, and ^{210}Pb is known to be deposited mainly from atmospheric fallout at a steady state, with little post-depositional mobility except for physical or biological mixing of the sediments[13,25]. However, global climate change, through increasing storm frequency and intensity, changes in the distribution of storm occurrences, and rising CO_2 levels in coastal waters could, directly and indirectly, impact seagrass C_{seq} rate estimations[26-29]. For example, since 95% of carbon in seagrass meadows is stored below ground in the sediments, decreases in sediment stabilisation and elevation functions are likely to affect carbon sequestration potential[30]. Conversely, sediment accretion rates in coastal ecosystems could respond to climate change through feedback that involves increased plant growth and production, through more efficient sediment trapping due to increased CO_2 levels[31] and sea-level rise[32].

Estuaries in southeast England, in particular, are among the most in danger from the cumulative effects of sea level rise and land subsidence, which could lead to a substantial shift in suitable habitat for seagrasses[33]. Furthermore, the lack of knowledge on the temporal relationship between seagrass degradation and loss and their ability to provide ecosystem services[30] highlights the need for research that incorporates historical assessments of variations in C_{seq} rates. Thus, active monitoring and management of seagrass ecosystems is required to improve the understanding of their ecology at a range of spatial and temporal scales in response to climate change forcing[34,35]. This study, therefore, presents an assessment of carbon sequestration rates from intertidal seagrass meadows in central Southern England, an assessment not previously undertaken for any UK seagrasses. The objectives were to: (1) investigate the use of ^{210}Pb dating methods to calculate sediment accretion rates for the studied sites; (2) to estimate carbon sequestration rates using standard and

conservative models; and (3) establish a relationship between dated horizons, carbon storage, sequestration, and environmental data.

METHODS

Study sites

Carbon sequestration rates were calculated from mixed, intertidal, seagrass meadows incorporating Zostera marina (Eelgrass) and Zostera noltii species, located in four study sites along the Solent coast of southern central England [Figure 1]: Creek Rythe (CRST) in Chichester Harbour; Hayling Island (LGST) and Farlington Marshes (FMST) in Langstone Harbour; and Porchester (PMST) in Portsmouth Harbour. Portsmouth, Langstone, and Chichester harbours are low-energy coastal environments, with a micro/meso-tidal range forming natural estuaries and harbours[36,37]. This region has some of the most complex tidal regimes in the U.K., caused by its natural coastal configuration and the proximity of a semi-diurnal tidal node in conjunction with historical natural and anthropogenically driven changes in water depth and coastal morphology, which has led to distortion of the tidal curve[38]. As a result, patterns of sediment transport in the region have been described as more complicated than other coastal regions along the UK, with fluvial and cliff erosion inputs, and transport driven by tides, wave activity, and littoral drift, generally moving from east to west[39-41] [Figure 1].

Field methods

During the summer of 2017 (June-August), two 50cm deep, 7.5 cm diameter PVC corers were used to extract sediment cores from within intertidal seagrass meadows at each of the four study sites, resulting in a total of eight cores (labelled CRST1, CRST 2, FMST1, FMST2, LGST1, LGST2, PMST1 and PMST 2). This chosen core depth was expected to cover the last 150 years of sediment accretion, which is the maximum detection limit for ^{210}Pb dating[42,43]. Sediment cores were carefully inserted into the sediment to allow minimal compression (< 10%)[25] and then carefully removed by digging around and capping at the bottom, to be immediately packed, labelled, and sealed with industrial cling film and duct tape, to prevent remobilisation, degradation, and contamination.

Laboratory methods

All cores were stored in freezers at -26 °C before preparation for laboratory analyses. Each frozen core barrel was extruded from the PVC tubes by allowing the outer core surface to thaw and then forcing the frozen sediment out. Sediment compaction was then re-assessed by measuring the length of the core section before and immediately after extrusion and no compaction was found[25]. Each sediment core was cleaned, logged, and sliced into 1 cm depth increment subsamples, to be analysed for ^{210}Pb, organic matter (converted to total organic carbon), sediment particle size, and soil bulk density[44,45].

Each 1 cm subsample was oven-dried at 40 °C prior to gamma spectrometry analysis, until a constant weight was achieved, to determine soil moisture content and dry bulk density[25]. Dried subsamples were then prepared for analysis by gently disaggregating the material using a pestle and mortar. Approximately 5-7 g of dried sediment from each subsample was carefully weighed into cylindrical plastic vials for determination of $^{210}Pb_{total}$ down core activities via gamma spectrometry[25]. The remaining dried sediment from each sample was separated to be analysed for organic matter content, to calculate carbon sequestration rates and particle size.

Gamma spectrometry

Each cylindrical plastic vial containing sediment sub-samples was placed in a Canberra well-type ultra-low background HPGe gamma-ray spectrometer to determine the activity of the ^{214}Pb (351.92 keV) and ^{210}Pb (46.54 keV). Spectral analysis was conducted using the Genie 2000 system. Energy and efficiency calibrations were carried out using bentonite clay spiked with a mixed gamma-emitting radionuclide

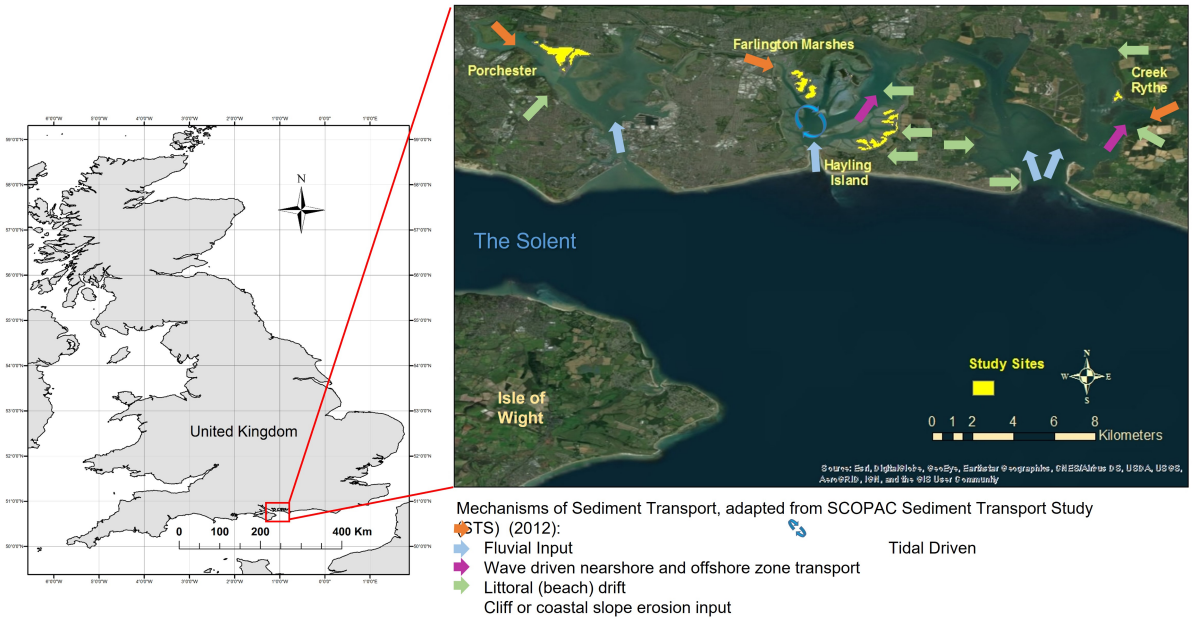

Figure 1. Map of the United Kingdom including a zoomed image showing the location of seagrass study sites in the Solent region (yellow), from west to east: Porchester (PMST), (Farlington Marshes (FMST), Hayling Island (LGST), and Creek Rythe (CRST). Coloured arrows show the patterns of sediment input and transport according to SCOPAC (STS)[40,41]. Maps are adapted from Esri ArcGIS online base maps, including scale bars in km.

standard, QCYK8163, and checked against an IAEA-certified sediment reference material (IAEA 135). To achieve maximum quality of data within a minimum time period, the samples were left counting until detection error was ≤ 5% for all the relevant radionuclides. Typically, each sample count time was between 48 and 96 h.

Organic matter content analysis

Oven-dried samples were weighed into individual beakers, 2-4 g for each sample, before being placed in the muffle furnace for loss in ignition (LOI) at 450 °C (selected temperature) for 24 h (selected exposure time)[46]. Samples were cooled at room temperature in a desiccator for at least one hour before weighing to determine the percentage of organic matter (% OM) following the protocols and equation used by previous studies analysing carbon stocks from the same sampling sites (Equation 1)[46,47]

$$OM = [(\text{dry mass before combustion (mg)} - \text{dry mass after combustion (mg)})/\text{dry mass before combustion (mg)}] * 100 \quad (1)$$

Sediment dry bulk density (Equation 2), carbon density, and organic carbon content (C_{org}) were also calculated[46,47].

$$DBD = (1 - \varphi) * 2.5 \quad (2)$$

where φ = porosity.

Values of C_{org} were calculated for core sections up to the maximum depth of detection of excess ^{210}Pb (reported in results) using equations derived from a previous study assessing carbon stocks on the same

sampling sites (Equation 3)[47].

$$\%C_{org} = -0.091 + 0.2881\ \%OM \quad (3)$$

Sediment carbon density was determined following C_{org} calculations (Equation 4)[46,47].

$$\text{Sediment Carbon Density } (g/dm^3) = [(\text{Dry mass (mg)} * \%C_{org})/\text{Dry mass (mg)}] * 100 \quad (4)$$

Particle size analysis

Following LOI, particle size analysis was carried out on all non-ground samples using a Malvern 2000 Laser Particle Size Analyser, graded according to the Wentworth scale[48], which was used to identify the silt and clay fractions to determine % mud content (% particles < 63 μm). Median grain size (D50, the particle size for which 50% of the distribution is finer or greater) and sorting coefficients (the degree of mixing of different grain sizes) were also calculated[49].

Radioisotope dating and sediment accretion rates

Excess (unsupported) ^{210}Pb was calculated as the difference between total ^{210}Pb and supported ^{210}Pb, to distinguish between excess ^{210}Pb deposited at the sediment surface and supported ^{210}Pb that has decayed in-situ. For the purpose of this study, ^{214}Pb levels have been used as a baseline to calculate supported ^{210}Pb. Cores were analysed in alternate 1-cm sections from the surface to the depth at which the excess ^{210}Pb concentration declined to zero. However, where a greater resolution was required, all 1cm samples were used.

In this study, short-term sediment accretion rates were determined for each core using the down-core distribution of ^{210}Pb with both the Constant Flux:Constant sedimentation (CF:CS) model and the constant rate of supply (CRS) model[50-52]. Although each ^{210}Pb model has specific assumptions, they share the following: (1) the deposition of unsupported ^{210}Pb is at a steady state; and (2) there is no post-depositional mobility of ^{210}Pb[14].

Constant flux: constant sedimentation (CF:CS) model

The CF:CS method involves calculating average sediment accretion rates for the sediment cores by dividing the decay constant of ^{210}Pb by the gradient of the log-normal line of the excess ^{210}Pb down the sediment core. In order to calculate the gradient of the line, a least squares regression analysis was used, and respective regression equations created. Sediment accretion rates were derived from the calculation below (Equation 5)[45]:

$$\text{Sediment accretion rates (cm/year)} = (\text{Decay constant } ^{210}\text{Pb})/(\text{Gradient of Ln line of the unsupported } ^{210}\text{Pb in the soil}) \quad (5)$$

where decay constant of ^{210}Pb = 0.03114.

Constant rate of supply

The Constant Rate of supply (CRS) model assumes a constant flux of ^{210}Pb to the sediments over time[53,54]. The initial specific activity is variable and inversely related to sediment accretion rates, as higher rates lead to lower $^{210}Pb_{excess}$ specific activity and vice versa. Dating is based on a comparison of $^{210}Pb_{excess}$ inventories below a given depth with the overall $^{210}Pb_{excess}$ inventory in the sediment core[14]. The accurate determination of the $^{210}Pb_{excess}$ inventories is of critical importance and required for the application of the CRS model[52].

Therefore, the CRS method was used to calculate accretion rates at specific dates. These were then linked to fluctuations in sediment supply by examination of available climate and hydrological data from the period established by the calculated dates. However, to guarantee a good fit to the data and calculation of the correct dates, the only sections included in the CRS calculations were the ones that showed a good fit to the data provided by the CF:CS regression lines.

The age of sediment at depth x was calculated using the formula below. The inventory of each sediment subsample was calculated using ^{210}Pb excess within the sample, multiplied by the dry bulk density of the sample. Ages (Equation 6) and hence sediment accretion rates (Equation 7) were then calculated using[51,52]:

$$\text{Age at depth x} = \frac{1}{(\text{decay constant of } 210\text{Pb})} \text{ x ln } \left(\frac{\text{unsupported inventory at depth x}}{\text{unsupported inventory at entire core}}\right) \quad (6)$$

$$\text{Sediment accretion rates (cm/year)} = (\text{Core section depth (cm)}/\text{Age at depth (x) - age at depth (x + 1)}) \quad (7)$$

Carbon sequestration rates

Sediment accretion rates calculated by the CRS model were used to calculate carbon sequestration rates, as a factor of dry bulk density (DBD) (Equation 2), soil organic carbon (%C_{org}) (Equation 3), and sedimentation rate (SR), per discrete layer (Equation 8)[22]:

$$\text{CSeq (g m}^{-2}\text{ year}^{-1}) = (\text{DBD (g cm}^{-3}) \times (\text{Corg(\%)}/100) \times (\text{SR (mm year}^{-1})/10)) * 10^{-4} \quad (8)$$

To account for the possibility of complex changes in flux, and the presence of labile, remineralised carbon in the surface layers, a conservative approach was also used to determine carbon sequestration rates (Equation 9)[55].

$$\text{CSeq (g m}^{-2}\text{ year}^{-1}) = (\text{DBD (g cm}^{-3}) \times (\text{lowest Corg(\%)in the core}/100) \times (\text{lowest SR that fits the data (mm year}^{-1})/10)) * 10^{-4} \quad (9)$$

Climate data

Historical climate data for the Solent region was obtained from the MET office archives, covering the period between 1900 and 2017 for daily maximum and minimum temperatures, wind speed, and precipitation. Daily values of maximum and minimum temperature, wind speed and precipitation were used to calculate a mean for each year of interest. Monthly sea level data were collected from the Permanent Service for Mean Sea Level (PSMSL) database for the Portsmouth station; data were available between 1955 and 2017. Monthly sea level values were used to calculate a yearly mean. The relationships between minimum and maximum temperature, wind speed, precipitation, sea level, and sediment C_{seq} rates (g m^{-2} year^{-1}) calculated using both the CRS and conventional methods were then analysed.

Statistical analyses

Spearman's Rho Correlation tests were used, due to the non-normal distribution of data, to assess the relationship between estimated C_{seq} rates (g m^{-2} year^{-1}) and the following variables: %mud, D50 (μm), sorting coefficient (φ), minimum, and maximum yearly average temperatures (°C), precipitation (mm), average wind speed (kn), and sea level (mm).

RESULTS

Radionuclide dating

Two cores, LGST 1 and PMST 2, had ^{210}Pb excess activity profiles indicating the occurrence of mixing or bioturbation and were, therefore, not used to calculate C_{seq} rates using the CRS model [Figures 2]. While both Creek Rythe cores had a comparable count value supporting ^{210}Pb equilibrium reached at 11.28 Bq/kg for CRST1 and 11.61 Bq/kg at CRST 2 [Figure 2A and B], core CRST 1 presented the highest surface count values of ^{210}Pb excess, of 128.76 Bq/kg [Figure 2A]. The cores from Farlington Marshes provided the lowest count values of supported ^{210}Pb at equilibrium, which were 7.84 and 7.24 Bq/kg for FMST 1 and FMST 2, respectively [Figure 2C and D]. The lowest surface ^{210}Pb excess count was similarly found in the FMST1 core, at 32.39 Bq/kg [Figure 2C]. The LGST cores had the highest maximum depth for ^{210}Pb excess activity detection (45 cm) [Figure 2E and F], and PMST 1 had the highest count values of supported ^{210}Pb at an equilibrium of 18.20 [Figures 2G].

Sediment accretion rates

The CF:CS model calculated regression between sediment accretion rates and depth revealed that the model was a good and statistical fit to the data from all cores ($P < 0.05$), with R^2 values ranging from 0.53 (PMST 2) to 0.94 (PMST 1) [Figure 2A-H]. The ^{210}Pb profiles' log-linear nature across all cores suggests steady accretion. According to the CF:CS model, the mean sediment accretion rates ranged from 1.2 mm year^{-1} (CRST 1 and FMST 1) and 10.8 mm year^{-1} (LGST 2) [Table 1]. For the CRST 1 and FMST 1 cores, the mean sediment accretion rates obtained by the CRS model were identical to those found using the simple CF:CS model, but higher than the CF:CS model for the PMST 2 core [Table 1]. Compared to CF:CS, all other cores' average sediment accretion rates calculated by the CRS method were lower [Table 1]. Similar to the CF:CS technique, the LGST 2 core had the highest sediment accretion rate of 6.3 mm year^{-1}, and the CRST 1 and FMST 1 cores CRS had the lowest rates of 1.2 mm year^{-1} [Table 1].

Carbon sequestration rates

Down-core profiles in $\%C_{org}$ displayed variable trends [Figure 3A-D], with some sites showing general declines in $\%C_{org}$ with depth, such as Creek Rythe and Porchester. For all sites, apart from Cowes, down-core distribution in $\%C_{org}$ was not monotonic, showing alternative increase and decrease with depth [Figure 3A-D]. Therefore, since $\%C_{org}$ calculation methods used in this study do not differentiate between buried and remineralised carbon, the uppermost 15 cm layer from each core was not considered for the calculation of C_{seq} rates using the CRS method. The mean $\%C_{org}$ calculated for all cores was 1.73 ± 0.46 (%), with cores from Farlington Marshes presenting the highest average downcore $\%C_{org}$, 2.30 ± 0.34 (%) in FMST 1 and 2.0 ± 0.25 (%) in FMST 2, while cores from Porchester presented the lowest downcore $\%C_{org}$ values, 1.49 ± 0.20 (%) in PMST 1 and 1.36 ± 0.29 (%) in PMST 2 [Figure 3].

C_{seq} rates were determined both by the conservative and ^{210}Pb CRS methods for all cores, apart from LGST 1 and PMST 2. For the conservative method, the lowest $\%C_{org}$ measured from each core was determined as follows: CRST 1, 0.88 (%); CRST 2, 1.43 (%); FMST 1, 1.84 (%), FMST 2, 1.58 (%); LGST 2 0.35 (%), PMST 1, 1.05 (%). Calculated C_{seq} rates by this method were remarkedly lower than the ones calculated by the CRS model for all cores [Table 2]. The average C_{seq} rate determined by using the conservative method was 15.38 ± 7.17 (g m^{-2} year^{-1}) [Table 2].

For all cores, the average C_{seq} rate determined by using the ^{210}Pb CRS method was 67.91 ± 32.39 (g m^{-2} year^{-1}) [Table 2]. In one of the cores from Hayling Island (LGST 2), the C_{seq} rates were highest at 106.05 ± 49.09 (g m^{-2} year^{-1}), and in Farlington Marshes (FMST 1), they were lowest at 19.91 ± 10.72 (g m^{-2} year^{-1}) [Table 2]. All cores presented sediments predominately muddy, fine and poorly

Table 1. Comparison between the average sediment accretion rates for Creek Rythe CRST 1 and CRST 2, Farlington Marshes FMST 1 and FMST2, Hayling Island LGST 1 and LGST 2, and Porchester PMST 1 and PMST 2. Sediment accretions rates market with an * are the ones used for the conservative method calculations

			Sediment accretion rates (mm year^{-1})		
Core	**Maximum ^{210}Pb excess activity (cm)**	**Method**	**Lower**	**Average**	**Upper**
CRST 1	15	CF:CS	0.6*	1.2	2.4
		CRS	-	1.2	-
CRST 2	19	CF:CS	2.5*	4.7	6.8
		CRS	-	3.6	-
FMST 1	11	CF:CS	0.6*	1.2	7.6
		CRS	-	1.2	-
FMST 2	13	CF:CS	1.1*	1.6	3.0
		CRS	-	1.2	-
LGST 2	45	CF:CS	8.8*	10.8	13.8
		CRS	-	6.3	-
PMST 1	11	CF:CS	1.2*	1.8	3.5
		CRS	-	1.7	-

sorted particles, with an average mud percentage (silt + clay) between cores of 86.80% ± 9.89%, a sorting coefficient of 1.97 ± 0.32 and a median particle size of 22.73 ± 7.96 (μm) [Table 2].

To assess the link between temperature and C_{seq} rates calculated by the CRS method, available daily temperature data from 1,900 were compiled at 12-h intervals (09:00 am-09:00 pm). In the analysed time period, the recorded annual maximum and lowest temperatures averaged 14.83 ± 0.23 (°C) and 7.53 ± 0.25 (°C), respectively [Table 2]. The analysis also included precipitation level data, with yearly averages of 2.18 ± 0.18 (mm) per day across all sites and collected during the same 12-h period each day [Table 2]. Daily maximum wind speed measurements were taken over the whole 24-h period, with an average of 9.69 ± 0.44 (kn) [Table 2]. The average reported sea level for the years under study was 7,074.01 ± 19.98 (mm) [Table 2].

In contrast to the CRST 2 core, where the oldest sediments were set down around 1947 [Figure 4B], the oldest sediments assessed for the CRST 1 core were laid down around 1906 [Figure 4A]. The oldest sediments in the FMST 1 core were deposited in approximately 1950 [Figure 4C], whereas the sediments in the FMST 2 core were older dated and had been deposited around 1939 [Figure 4D]. The dateable section in the core from the Porchester site was substantially younger, with the PMST 1 core having a maximum age of 1972 [Figure 4E]. The oldest section was 1921, found in the LGST 2 core [Figure 4F]. These were all revealed by ^{210}Pb dating using the CRS method.

For all sediment cores, the %mud increased through time [Figures 5A, 6A, 7A, 8A]. The lowest % of mud was recorded at the surface of the FMST 2, rising from 57.35% in 2017 to 63.79% about 1939 [Figure 6A]. In comparison to all other cores, the %mud for the LGST 2 core showed a considerable variance with age, moving from 77.78% in 2017 to the maximum value of 94.25% for this core than all other cores, changing around both 1994 and 1999 [Figure 7A]. Conversely, the %mud for the PMST 2 core had little variance throughout time, ranging from 94.70% around 2017 to 93.76% around 1954 [Figure 8A]. Although more recent sediments were generally better sorted than older ones for all cores, all sediment layers were classed as being poorly or very poorly sorted [Figures 5B, 6B, 7B, 8B]. For the Hayling Island (LGST 1 and 2) and Porchester (PMST 1 and 2) cores, the degree of sorting followed the same patterns of change with time as %mud [Figure 7B].

Table 2. Depth and age of all collected cores, with respective carbon sequestration rates, %mud, median grain size (D50), degree of sorting, and climate data including maximum and minimum temperature ranges, precipitation levels, and wind speed (MET office archives - since 1900), as well as mean sea level (Permanent Service for Mean Sea Level (PSMSL) database - Portsmouth station). Values are presented as mean (±SD) for all variables. Mean values for all cores are presented in bold

Sites	Core	Core depth (cm)	Core age	C_{seq} rate - CRS (g m^{-2} $year^{-1}$)	C_{seq} rate - conservative (g m^{-2} $year^{-1}$)	%Mud	D50 (μm)	Sorting coefficient (φ)	$Temp_{max}$ (0900-0900) (°C)	$Temp_{min}$ (0900-0900) (°C)	Precipitation (0900-0900) (mm)	Windspeed (0100-2400) (kn)	Sea level (mm)
Creek Rythe (CRST)	1	12.5	1906-2016	24.56 ± 19.42	3.98 ± 0.59	92.49 ± 5.61	23.64 ± 10.10	1.93 ± 0.75	14.71 ± 0.34	6.99 ± 0.51	2.22 ± 0.34	8.16 ± 2.42	7,082.0 ± 50.91
	2	16.5	1947-2016	86.22 ± 98.82	23.91 ± 4.15	83.31 ± 11.74	27.60 ± 11.77	2.41 ± 0.21	14.90 ± 0.45	7.41 ± 0.66	1.83 ± 0.31	10.26 ± 1.16	7,066.1 ± 37.91
Farlington Marshes (FMST)	1	10.5	1950-2017	19.91 ± 10.72	11.30 ± 3.02	94.29 ± 3.44	16.64 ± 4.52	2.19 ± 0.22	15.10 ± 0.72	7.95 ± 1.20	2.39 ± 0.15	10.13 ± 1.06	7,083.0 ± 39.64
	2	12.5	1939-2017	51.07 ± 27.55	13.82 ± 6.07	67.31 ± 13.18	37.54 ± 10.64	1.66 ± 0.17	14.89 ± 0.49	7.49 ± 0.61	2.27 ± 0.37	8.83 ± 2.01	7,078.5 ± 24.72
Hayling Island (LGST)	1	36.5	-	-		96.28 ± 3.47	12.95 ± 1.50	2.42 ± 0.21	14.51 ± 0.87	7.17 ± 0.87	2.26 ± 0.58	9.57 ± 0.25	7,067.5 ± 39.31
	2	44.5	1921-2017	106.05 ± 49.09	19.47 ± 4.72	86.26 ± 7.50	21.03 ± 5.96	2.48 ± 0.06	14.87 ± 0.73	7.36 ± 0.74	2.07 ± 0.42	9.85 ± 0.78	7,054.8 ± 37.94
Porchester (PMST)	1	8.5	1972-2017	76.70 ± 95.08	8.79 ± 0.51	79.72 ± 12.09	26.68 ± 7.74	1.24 ± 0.36	14.51 ± 0.62	7.50 ± 0.58	2.12 ± 0.30	9.81 ± 1.03	7,062.5 ± 33.93
	2	24.5	-	-		94.79 ± 0.85	15.77 ± 1.54	1.42 ± 0.58	14.76 ± 0.73	7.51 ± 0.62	2.13 ± 0.58	9.55 ± 0.52	7,061.7 ± 41.77
Mean				**67.91 ± 32.39**	**15.38 ± 7.17**	**86.81 ± 9.81**	**22.73 ± 7.96**	**1.97 ± 0.32**	**14.78 ± 0.20**	**7.42 ± 0.28**	**2.16 ± 0.17**	**9.52 ± 0.70**	**7,069.5 ± 10.43**

Sediment accretion rates ranged from 0.5 to 2.6 mm $year^{-1}$, between 1906 and 2016, for the CRST 1 core, peaking at 1906 (2.6 mm $year^{-1}$) and 1975 (1.2 mm $year^{-1}$) [Figure 5C]. While sediment accretion rates for the CRST 2 core ranged from 0.76 to 1.99 mm $year^{-1}$, between 1947 and 2016, peaking in 1982 (12.1 mm $year^{-1}$), and 1980 (4.9 mm $year^{-1}$) [Figure 5C]. The Farlington Marshes FMST 1 core had the highest accretion rates reported around 1984 (2.22 mm $year^{-1}$), ranging from 0.43 to 1.37 mm $year^{-1}$ between 1950 and 2017 [Figure 6C]. Moreover, sediment accretion rates for the FMST 2 core indicated an overall trend of rise through time, with a standstill during the 1950s and 1990s and greater accretion rates reported around 2017 (2.21 mm $year^{-1}$) and 2007 (1.65 mm $year^{-1}$) [Figure 6C]. In general, sediment accretion rates decreased with age for the LGST 2 core, ranging from 0.77 to 6.50 mm $year^{-1}$, between 1921 and 2017 [Figure 7C]. For the Porchester, PMST 1 core, accretion rates varied between 0.82 to 2.37 mm $year^{-1}$, between 1972 and 2017 [Figure 8C].

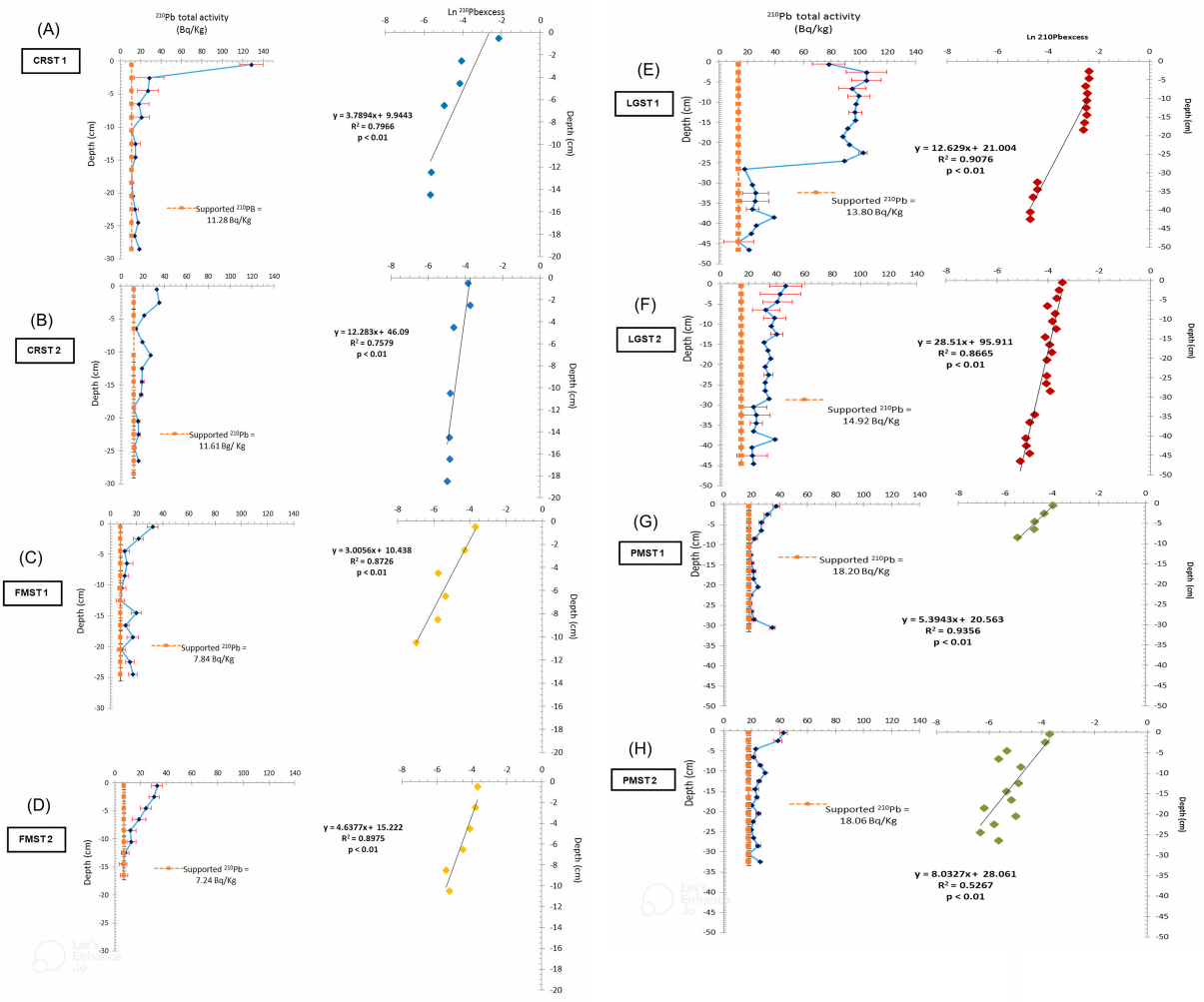

Figure 2. (A-D) Total activity down-core for ^{210}Pb (A) CRST 1, (B) CRST 2, (C) FMST 1, and (D) FMST 2 represented by blue lines (diamond markers), with error calculations (5%) shown in red. Supported ^{210}Pb values represented by orange (square markers) lines on all graphs, on the left. Respective graphs on the right showing the Natural Log (Ln) of ^{210}Pb excess per depth (CF:CS model) with regression equations. (E-H) Total activity down-core for ^{210}Pb (E) LGST 1, (F) LGST 2, (G) PMST 1, and (H) PMST 2 represented by blue lines (diamond markers), with error calculations (5%) shown in red. Supported ^{210}Pb values represented by orange (square markers) lines on all graphs, on the left. Respective graphs on the right show the Natural Log (Ln) of ^{210}Pb excess per depth (CF:CS model) with regression equations.

The greatest CRS calculated C_{seq} rate for the Creek Rythe, CRST 1 core, was recorded in 1930 at 35.68 g m^{-2} year^{-1}, while the lowest was recorded in 2016 at 10.3 g m^{-2} year^{-1} [Figure 5D]. Comparatively, the CRST 2 core showed higher C_{seq} rates, with the highest value occurring in 1982 at 296.5 g m^{-2} year^{-1}, and the lowest in 1947 at 18.6 g m^{-2} year^{-1} [Figure 5D]. The Farlington Marshes FMST 1 core's CRS calculated C_{seq} rates ranged from 7.31 in 1950 to 35.38 g m^{-2} year^{-1} in the years surrounding 1984, while C_{seq} rates for the FMST 2 core showed maximum values of 81.03 g m^{-2} year^{-1}, presented around 1958, and the lowest of 12.36 g m^{-2} year^{-1} shown around 1939, demonstrating substantial oscillations over the dated time period and not following the same pattern as sediment accretion rates in this core [Figure 6D]. The LGST 2 core recorded the highest values around 1956, at 184.80 g m^{-2} year^{-1}, and the lowest values around 1921, at 15.57 g m^{-2} year^{-1}, showing contrasting patterns to sediment accretion rates [Figure 7D]. For the Porchester PMST 1 core, in addition to declining with age, CRS calculated C_{seq} rates have been declining more recently

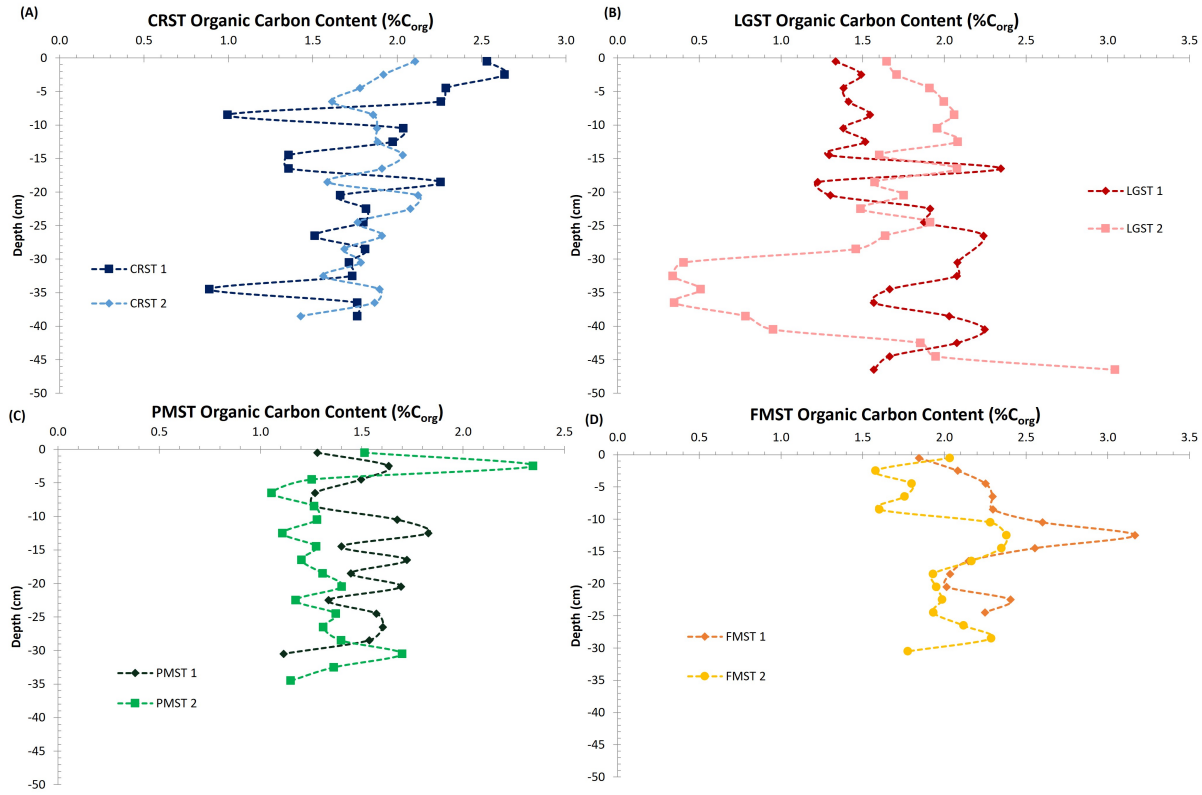

Figure 3. Down-core profile of %C_{org} for (A) CRST, (B) LGST, (C) PMST, and (D) FMST sampling sites.

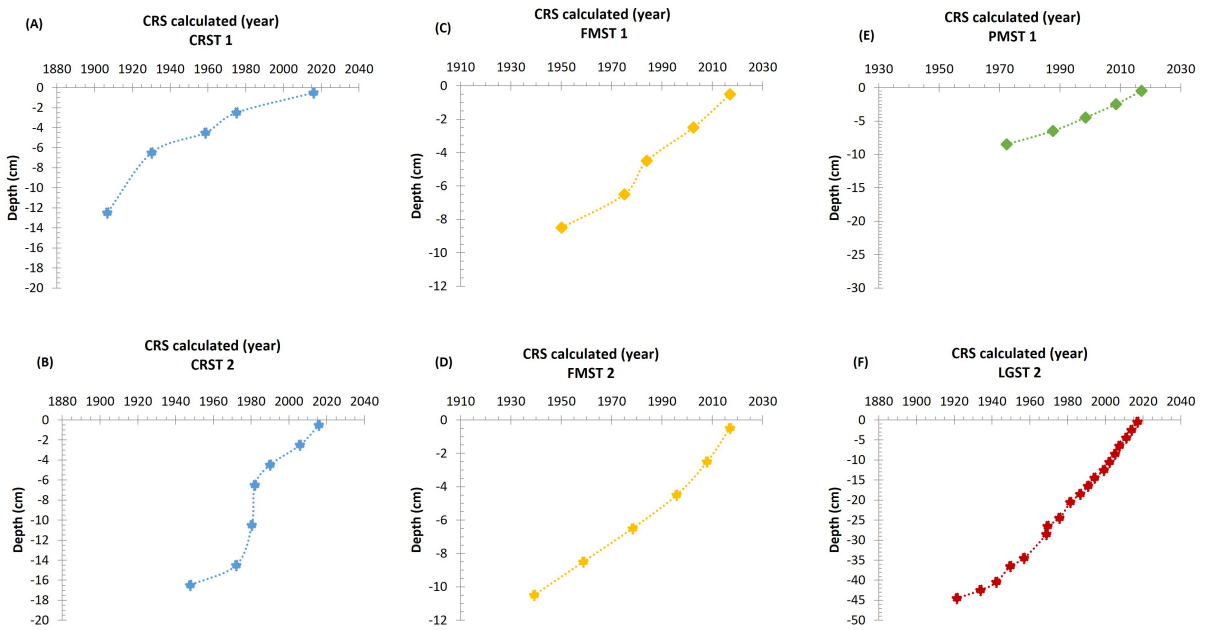

Figure 4. CRS calculated the age of each depth for the (A) CRST 1, (B) CRST 2 cores for the Creek Rythe site, (C) FMST 1, (D) FMST 2 cores for the Farlington Marshes site, (E) PMST 1, for the Porchester site and (F) LGST 2 for the Hayling Island site.

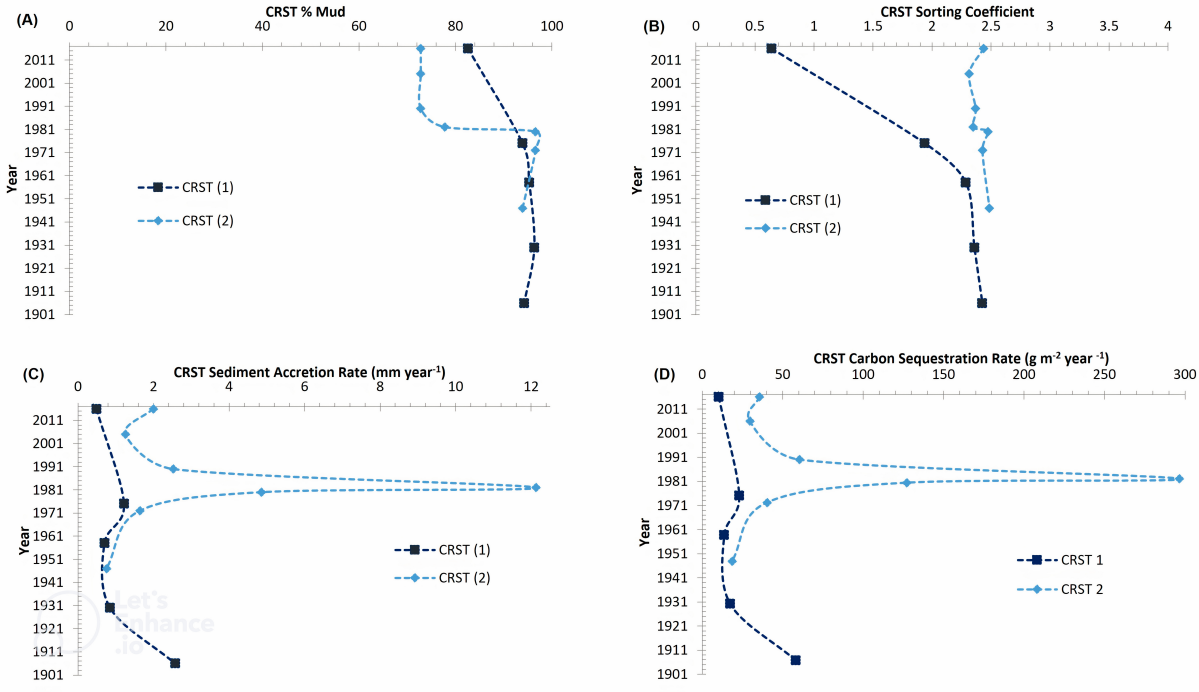

Figure 5. Distribution of % mud (A), Degree of sorting (B), ^{210}Pb CRS method derived sediment accretion rates (C), and Carbon sequestration rates (D), with age, for the CRST 1 and 2 cores.

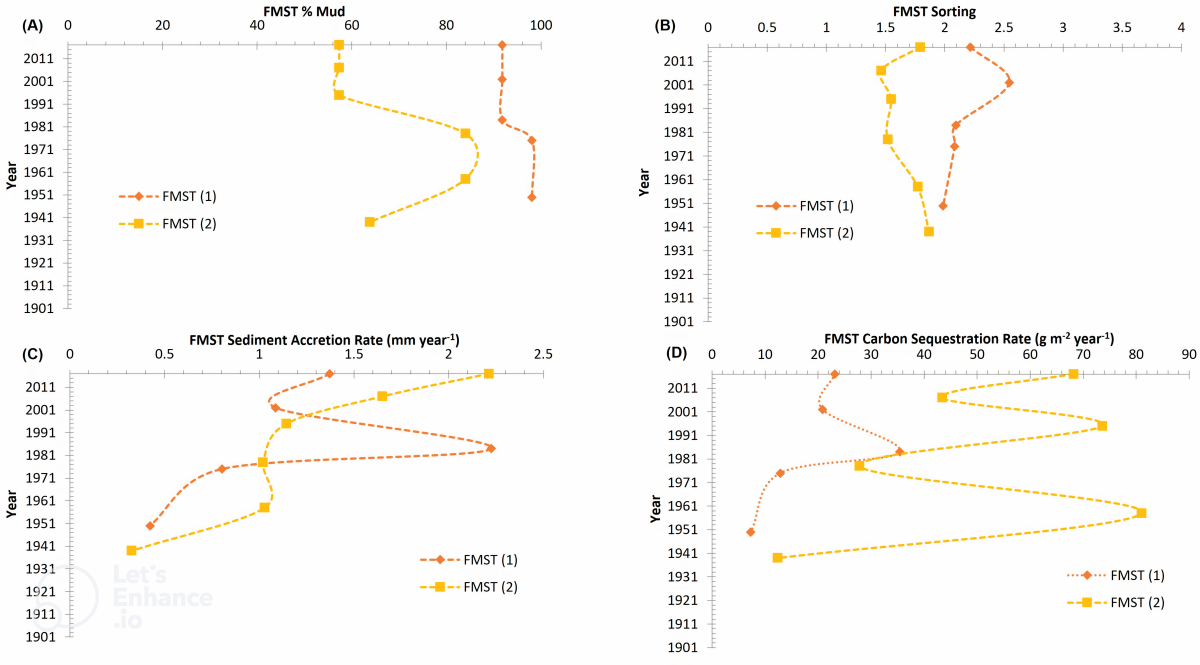

Figure 6. Distribution of % mud (A), Degree of sorting (B), ^{210}Pb CRS method derived sediment accretion rates (C), and Carbon sequestration rates (D) with age, for the FMST 1 and 2 cores.

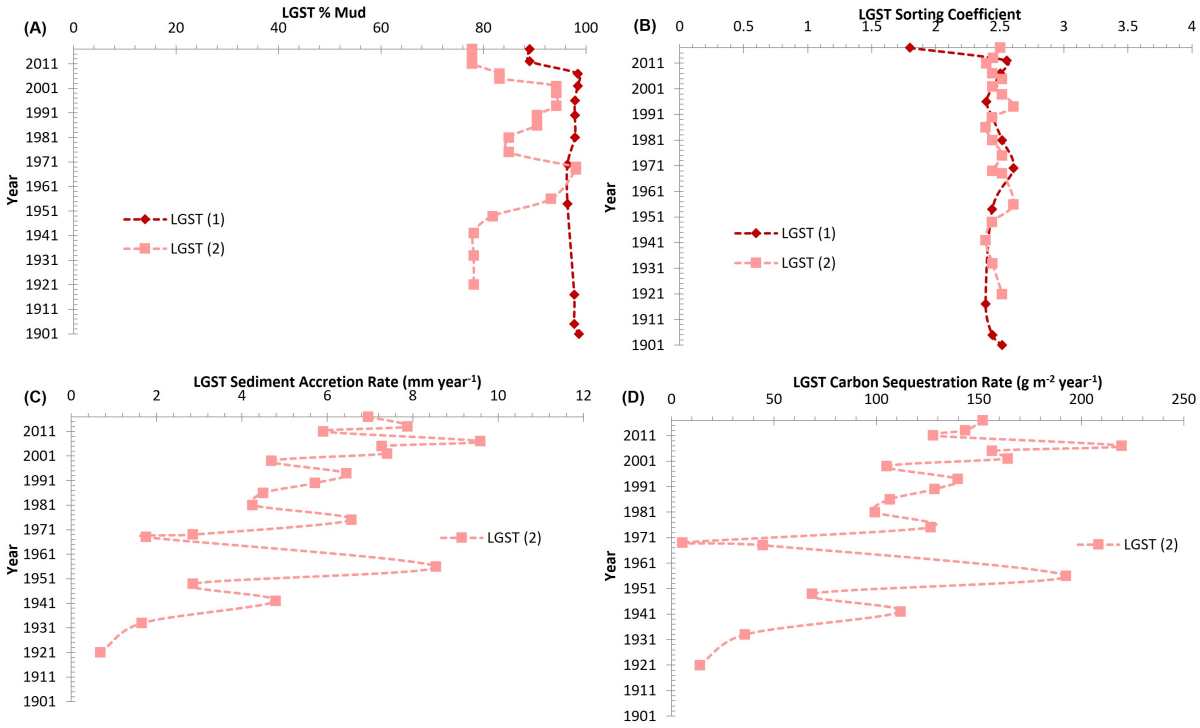

Figure 7. Distribution of % mud (A) and degree of sorting, (B) for the LGST 1 and 2 cores, ^{210}Pb CRS method derived sediment accretion rates (C), and Carbon sequestration rates (D) with age, for the LGST 2 core.

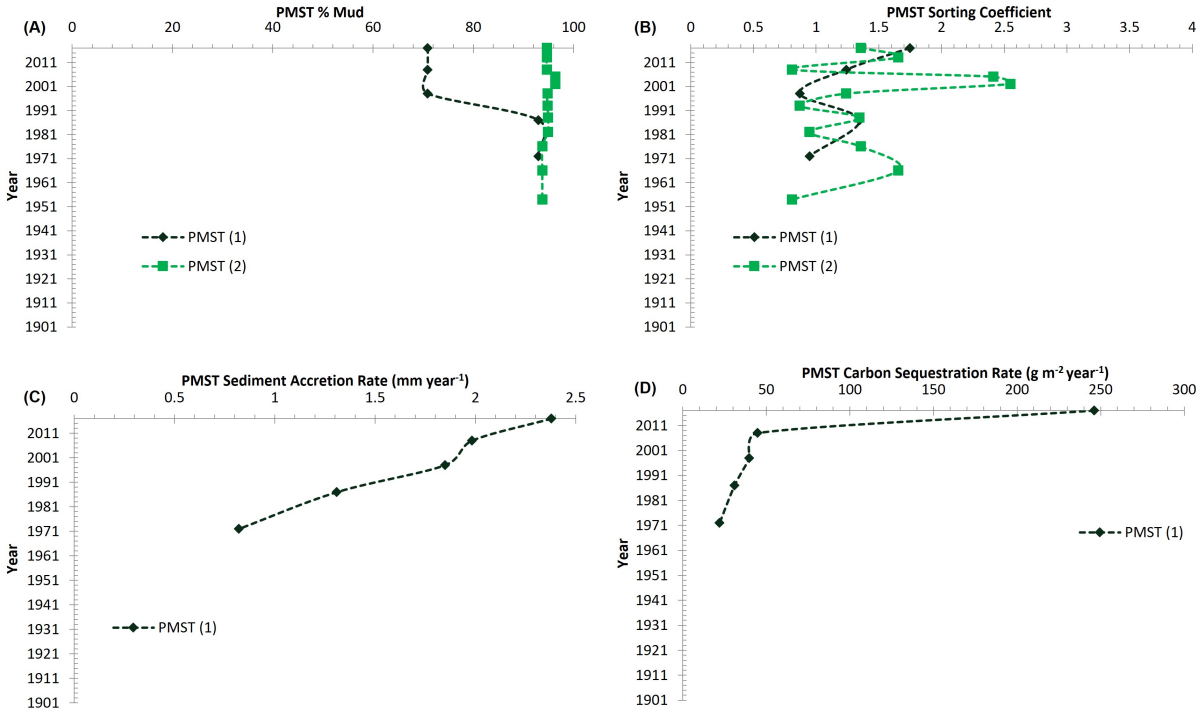

Figure 8. Distribution of % mud (A), Degree of sorting (B) for the PMST 1 and 2 cores, ^{210}Pb CRS method derived sediment accretion rates (C), and Carbon sequestration rates (D) with age for the PMST 1 core.

than sediment accretion rates, up until 2010, peaking in 2017 at 246.08 g m^{-2} $year^{-1}$ and reaching their lowest level in 1972 at 22.02 g m^{-2} $year^{-1}$ [Figure 8D].

Relationships between environmental variables and carbon sequestration rates

C_{seq} rates calculated by both the CRS [Table 3] and conventional methods [Table 4] demonstrated no significant relationships for most sampling sites. Precipitation levels showed a negative effect on carbon sequestration processes calculated by the conventional method in Creek Rythe's cores (CRST), as can be seen from the significant negative relationship between the two variables (r_s = -0.757; $P < 0.05$) [Table 4].

DISCUSSIONS

Radiometric dating

This study estimated sediment accretion rates from seagrass sediment cores in the Solent region, U.K. using ^{210}Pb activity. The similar accretion rates seen across all cores when measured by the CF:CS and CRS methods provide evidence that these methods apply to the study area. However, there were variations in the maximum depth of $^{210}Pb_{excess}$ detection, sediment accretion rates, and C_{seq} rates between cores from the same study sites when calculated using the CRS method. Results also showed large differences between C_{seq} rates calculated by the CRS and the conventional approach, which indicate the need for further direct and local measurements of C_{seq} rates, using reliable methods and mathematical models, rather than using global or regional estimations for blue carbon budgets.

The use of ^{210}Pb to assess sediment accretion rates

The CRS method utilised in this study has been widely applied in estuarine and vegetated coastal environments due to its robustness against non-monotonic features in the ^{210}Pb record and is assumed to be relatively insensitive to mixing[43,53,56,57]. The model assumes a constant direct ^{210}Pb atmospheric fallout, combined with fluctuations in the sedimentation rate and variable initial specific activity, calculated in combination with sediment accumulation rates, which may occur in response to natural processes or anthropogenic influences[58]. Moreover, the CF:CS model is also, to some degree, able to cope with temporal variations in mass accumulation rates, such as mixing at the surface layers[14]. Arias-Ortiz *et al.* listed seven distinct types of $^{210}Pb_{excess}$ specific activity profiles that can be identified in vegetated coastal sediments based on a review of the literature[14]. These types have been classified in terms of "ideal" profiles, produced by constant sediment accumulation in steady-state conditions, and ones that would show one or more of the most common disturbances encountered in vegetated coastal sediments[14]. The most common disturbances listed are the presence of mixing (physical or bioturbation), increasing sediment accumulation rates, erosion, or alteration by intrinsic features of sediments such as heterogeneous grain size, distribution, and decay of organic matter. Based on this classification, the sediment cores from Hayling Island (LGST 1 and 2) and Creek Rythe (CRST 1 and 2) showed $^{210}Pb_{excess}$ specific activities that possibly correspond to mixing attributed to higher rates of sediment accretion[59-62], and mixing as a result of bioturbation or sediment resuspension (CRST 1, LGST 1)[14,21,35,63,64]. More specifically, the CRST 2 core displayed a $^{210}Pb_{excess}$ activity profile consistent with the deposition of allochthonous older material[65]. Moreover, the Porchester PMST 1 core showed a scattered $^{210}Pb_{excess}$ activity profile, which might reflect the periodic occurrence of mixing, resuspension, and allochthonous input, causing repetitive reworking in the overall mixed sediment column[21,66]. Most cores presented $^{210}Pb_{excess}$ activity profiles consistent with erosion processes, except the CRST 2 core from Creek Rythe and LGST 2 core from Hayling Island[13,21,67]. Ideally, additional cores would be needed to identify possible patterns of erosion, mixing, or disturbance on the sediment profiles from the sampled sites. However, given the large agreement in accretion rates calculated by both methods and the good fit to the data presented by the CF:CS method, ^{210}Pb activity profiles have been deemed a worthy method to provide this initial assessment of sediment accretion rates for the sampled sites.

Table 3. Spearman's correlation coefficients (rs) between CRS calculated Cseq rates and environmental variables for all study sites

Environmental variables / Sampling sites	%MUD	D50 (μm)	Sorting coefficient (φ)	Temp max (0900-0900) (°C)	Temp min (0900-0900) (°C)	Precipitation (0900-0900) (mm)	Wind speed (0100-2400) (kn)	Sea level (mm)
Creek Rythe (CRST)	0.474	0.062	0.225	0.050	0.186	-0.226	0.266	0.238
Farlington Marshes (FMST)	-0.556	0.570	-0.490	0.265	0.163	-0.201	-0.601	-0.067
Hayling Island (LGST)	-0.007	-0.004	0.163	-0.177	0.208	0.338	-0.188	0.427
Porchester (PMST)	-0.482	0.482	0.832	0.636	0.599	0.909	-0.281	0.819

Table 4. Spearman's correlation coefficients (rs) between conventional method calculated Cseq rates and environmental variables for all study sites. Statistically significant relationships are in bold, represented by * when *P* < 0.05

Environmental variables / Sampling sites	%MUD	D50 (μm)	Sorting coefficient (φ)	Temp max (0900-0900) (°C)	Temp min (0900-0900) (°C)	Precipitation (0900-0900) (mm)	Wind speed (0100-2400) (kn)	Sea level (mm)
Creek Rythe (CRST)	-0.37	0.162	0.344	0.184	0.286	**-0.757***	0.513	-0.636
Farlington Marshes (FMST)	-0.195	0.131	-0.381	-0.504	-0.517	0.151	-0.075	-0.523
Hayling Island (LGST)	-0.397	0.413	0.143	0.035	0.039	-0.153	0.296	0.285
Porchester (PMST)	-0.676	0.676	0.143	0.438	0.222	0.083	0.471	0.622

Sediment accretion and C_{seq} rates

Sediment accretion rates calculated for most sites, by both the CRS and CF:CS methods, ranged from 0.61-6 mm year^{-1}, agreed with the reported global range of 2.02 ± 0.44 mm year^{-1}[68]. However, Hayling Island's LGST 2 core was the only exception, producing higher average accretion rates of 6.3 mm year^{-1}, using the CRS method, and 10.8 mm year^{-1}, using the CF:CS method. Moreover, this study's mean sediment accretion rates were generally higher than those reported for Western Australia's *Posidonia australis* meadows by Marba *et al.*[13], of 0.67 ± 0.03 mm year^{-1}, and for temperate, tropical and sub-tropical multi-species seagrass meadows along East and Southeast Asia, by Miyajima *et al.*,[20] of between 0.32-1.34 mm year^{-1}. Most study sites, apart from Hayling Island, had cores with calculated accretion rates similar to those reported by Jankowska *et al.*[62] (1.3 ± 0.2 mm year^{-1}) and Poppe and Rybczyk[3] (1.9 ± 0.1 mm year^{-1}) for *Z. marina* meadows. However, Porchester and Creek Rythe also presented cores with higher mean sediment accretion rates, comparable to Mediterranean *Posidonia oceanica* meadows, of between 2.4-4.2 mm year^{-1}[19], demonstrating the variability in sediment accretion within sites.

The measured supported ^{210}Pb ranged from 7.24 Bq kg^{-1} in Farlington marshes (FMST 2 core) to 18.20 Bq kg^{-1} in Porchester (PMST 1). Not too different from the ones described by a previous study, analysing salt marshes within the Solent region, of 12.2 Bq kg^{-1} supported ^{210}Pb on average[38]. Sites presenting low sediment deposition would show a ^{210}Pb inventory lower than expected, and bioturbation would be responsible for the apparent long-term accretion rate, while a higher-than-expected inventory could imply that the site is depositional, and the apparent long-term accretion rate reflects both bioturbation and accretion[3,59,69,70]. Results from this study support these assumptions, with higher sediment

accretion rates found in Porchester (PMST 1), of 4.2- and 4.3-mm year^{-1}, than Farlington Marshes (FMST 2), of 1.6- and 1.2-mm year^{-1}, when calculated by both the CRS and CF:CS methods, respectively. This is because, despite the input of fluvial sediment in both sites, Porchester is less exposed to tidally driven sediment mixing than Farlington Marshes, which could explain the lower sediment accretion rates, possibly caused by sediment flushing [Figure 1][41].

Patterns of %C_{org} profiles for all sediment cores from this study were non-monotonic, potentially representing the surface mixed layer where bioturbation processes often occur[55]. However, it is important to highlight that even though the approach taken by the CRS method used in the study does not take erosion/bioturbation and remineralisation into account, and there is no differentiation between autochthonous and allochthonous carbon, the study aimed to provide an initial estimation of C_{seq} processes in the study region[55]. Mean C_{seq} rates, calculated by the CRS method, from seagrass meadows in the studied sites, of 75.12 g m^{-2} year^{-1}, were comparable to other global regions[67]. Furthermore, a review of seven studies summarising a total of 123 sites, reported an estimated range of C_{seq} rates from 45 to 190 g m^{-2} year^{-1}, even though the mean calculated rate of 138 ± 38 g m^{-2} year^{-1} was higher than the one reported in this study[9]. Conversely, the mean C_{seq} rates from the Solent's seagrass meadows are similar to those reported by Jankowska *et al.*, from *Z. marina* meadows in the Baltic Sea[62]. The mean C_{seq} rates calculated by the conventional method, of 15.38 g m^{-2} year^{-1}, were much lower than the mean CRS C_{seq} rate for the studied sites, and reported global ranges, suggesting possible underestimation. Moreover, an increase in C_{seq} rates over time is usually described by studies investigating restored seagrass sites[13,67]. For example, Marba *et al.* reported an increase in C_{seq} rate from 16.2 ± 2.4 to 25.2 ± 4.7 g m^{-2} year^{-1}[13], between 6-year and 18-year restored seagrass sites from Oyster Harbour, Australia, with C_{seq} rates values much closer to the ones calculated by the conventional method in this study. This is relevant since it has been reported that the seagrass meadows in this study are likely to still be in a recovery phase after reported dieback caused by wasting disease[71,72]. Previous studies have highlighted historical limitations of global seagrass C_{seq} rate assessments, mainly based on limited data or the use of indirect approaches[73,74]. Studies also call attention to the large, and yet understudied, variability in seagrass C_{seq} potential, and the need for preliminary and baseline regional assessments, such as the one presented by this study, despite their limitations[74].

Influence of environmental variables and climate events on C_{seq} rates

The wide range in estimated C_{seq} rates by seagrasses is usually associated with their high net production variability, including variability among species and habitats, and methods used[6,7,11,55]. However, some studies suggest that the variability in C_{seq} rates may be a consequence of difficulties in estimating reliable long-term accretion rates from these environments, with most reviews usually being dominated by species like *Posidonia oceanica* and *Zostera marina*[3,55,75]. Moreover, environmental factors, extreme weather events, and anthropogenic impacts can influence C_{seq} rates between sampling sites in different ways. For example, an analysis of the CRS accretion rates per calculated date for the LGST 2 core in Hayling Island showed a large peak in accretion around 1970-1980, which did not correspond to a similar peak in C_{seq} rates. This suggests that there was a large input of mineral sediment during that period, possibly due to coastal erosion from a reported storm (1979), recorded coastal flood events (1981), and natural littoral drift in the area[40-41].

Both cores from Creek Rythe showed very similar patterns of sediment accretion and C_{seq} rates over time, with peaks around the 1980s when calculated by the CRS method. These could be related to the reported periods of high wind speeds, as well as the occurrence of storms and floods during this period[76]. However, cores from the other sites showed variations in this pattern; for example, one of the cores from Farlington Marshes (FMST 2) showed two peaks in C_{seq} rates around 1995 and 1955, even though sediment accretion rates were declining during these periods. These fluctuations could be related to the increase in %mud recorded for the same period, around 1995, preceded by a decrease around 1955, with closely related sorting

patterns. This would also corroborate the notion that seagrass meadows in central southern England are still in a recovery phase and have not attained the levels of canopy density and carbon storage capacity recorded before the 1950s global dieback[72]. Porchester's PMST 1 core showed a steep increase in C_{seq} rates over the last decade, which is likely to be related to the higher % of mud found in the top layers of the core and an increase in allochthonous organic matter input by anthropogenic activities including urban development.

Several studies have reported evidence of climate-induced shifts in the seasonal growing pattern of marine primary producers[32,77-80]. This would be increasingly probable if a cyclone or severe storm passed over already highly fragmented seagrass beds[29,81,82]. Shields *et al.* related this shift to an increase in the length of the stressful summer season, impacting the timing of *Z. marina's* growth and decline periods[34]. Gentle increases in temperature enhance the rate of photosynthesis and primary production, which could promote seagrass growth, increasing meadow extent and, therefore, trapping more suspended particles, increasing C_{seq} rates[83-86]. Conversely, temperature stress on seagrasses might result in distribution shifts, changes in patterns of sexual reproduction, altered seagrass growth rates, and metabolism, and changes in their carbon balance, which will cause plants to die[1]. Lower temperatures, however, could negatively impact the seagrass growth rate, promoting dieback during wintertime, which could then increase C_{seq} rates by increasing the input of autochthonous carbon[84,87,88]. An adverse impact of heavy rain, associated with storm events like the ones described in this study, is the decrease in salinity levels due to increased freshwater runoffs, causing large-scale losses of seagrass habitats that might take several years to recover[89,90]. Anthropogenic or natural disturbance of seagrass meadows may decrease canopy height and density by damaging plants, as well as uprooting plants in some parts of the bed, resulting in the fragmentation of the meadow into patches[91]. After an intense storm, it is typical to find dead seagrasses piled up in extensive wrack lines along the shore[75]. Seagrass loss also results from smothering by sediments and light limitation due to increased turbidity from suspended sediments[78]. These dieback events, promoted by extreme weather, can temporarily enhance sediment C_{seq} rates, due to the increase in organic matter from seagrass decay within the meadow and neighbouring areas[23]. In contrast, if disturbances are too intense or prolonged, seagrass fragments may keep decreasing into smaller units until they disappear completely[91]. However, due to their unexpected nature and unpredictability, the consequences of extreme climate events on seagrass communities can be incredibly challenging to monitor[91], highlighting the need to monitor seagrass meadows regularly to measure their status and record short and long-term trends and possible effects of disturbance on these ecosystems, to establish reliable C_{seq} rates[20,76].

CONCLUSIONS

The calculated carbon sequestration rates from seagrass meadows in central south England confirm the significance of these ecosystems as blue carbon sinks, on a par with other global areas, including tropical sites. However, variations in seagrass carbon sequestration rates are correlated with sediment properties as well as environmental variables and, most importantly, methods used. Furthermore, the difference in $^{210}Pb_{excess}$ activity profiles recorded from the studied sites, and resulting sediment accretion rates, highlight the variation in the potential carbon sequestration rate potential between meadows and the need for direct measurements to be reported rather than extrapolations based on reported values for other areas. Monitoring of the condition and extent of seagrass meadows is crucial, particularly in light of the predicted increased frequency and magnitude of climate change-related events.

DECLARATIONS

Authors' contributions

Made substantial contributions to the conception and design of the study and performed data analysis and interpretation: do Amaral Camara Lima M, Ward RD

Performed data acquisition, as well as providing administrative, technical, and material support: Joyce CB

Availability of data and materials

An indication that the data supporting the conclusions can be provided upon reasonable request to the corresponding author.

Financial support and sponsorship

None.

Conflicts of interest

All authors declared that there are no conflicts of interest.

Ethical approval and consent to participate

Not applicable.

Consent for publication

Not applicable.

REFERENCES

1. Björk M, Short F, Mcleod E, Beer S. Managing seagrasses for resilience to climate change. Gland, Switzerland: IUCN; 2008, 56p. Available from: https://www.preventionweb.net/files/9648_20080241.pdf [Last accessed on 28 Sep 2023].
2. Nellemann C, Corcoran E, Duarte CM, et al. Blue carbon: the role of healthy oceans in binding carbon: a rapid response assessment. 2009. Available from: https://policycommons.net/artifacts/1375378/blue-carbon/1989638/ [Last accessed on 28 Sep 2023].
3. Poppe KL, Rybczyk JM. Carbon sequestration in a pacific northwest eelgrass (*Zostera marina*) meadow. *Northwest Sci* 2018;92:80-91. DOI
4. Bouwer L, Capriolo A, Chiabai A, et al. Chapter 4 - upscaling pscaling the impacts of climate change in different sectors and adaptation strategies. In: Adapting to Climate Change in Europe. Elsevier; 2018. pp. 173-243. DOI
5. Alongi DM. Current status and emerging perspectives of coastal blue carbon ecosystems. *Carbon Footprints* 2023;2:12. DOI
6. Grimsditch G, Alder J, Nakamura T, Kenchington R, Tamelander J. The blue carbon special edition - Introduction and overview. *Ocean Coast Manag* 2013;83:1-4. DOI
7. Lavery PS, Mateo MÁ, Serrano O, Rozaimi M. Variability in the carbon storage of seagrass habitats and its implications for global estimates of blue carbon ecosystem service. *PLoS One* 2013;8:e73748. DOI PubMed PMC
8. Rozaimi M, Serrano O, Lavery PS. Comparison of carbon stores by two morphologically different seagrasses. *J R Soc West Aust* 2013;96:81-3. Available from: https://www.proquest.com/openview/3648688ca12e53c5b5a4f805d1026548/1?pq-origsite=gscholar&cbl=136100 [Last accessed on 28 Sep 2023]
9. Mcleod E, Chmura GL, Bouillon S, et al. A blueprint for blue carbon: toward an improved understanding of the role of vegetated coastal habitats in sequestering CO_2. *Front Ecol Environ* 2011;9:552-60. DOI
10. Serrano O, Gómez-López DI, Sánchez-Valencia L, et al. Seagrass blue carbon stocks and sequestration rates in the Colombian Caribbean. *Sci Rep* 2021;11:11067. DOI PubMed PMC
11. Garrard SL, Beaumont NJ. The effect of ocean acidification on carbon storage and sequestration in seagrass beds; a global and UK context. *Mar Pollut Bull* 2014;86:138-46. DOI PubMed
12. Zhong C, Li T, Bi R, et al. A systematic overview, trends and global perspectives on blue carbon: a bibliometric study (2003-2021). *Ecol Indic* 2023;148:110063. DOI
13. Marbà N, Arias-ortiz A, Masqué P, et al. Impact of seagrass loss and subsequent revegetation on carbon sequestration and stocks. *J Ecol* 2015;103:296-302. DOI
14. Arias-Ortiz A, Masqué P, Garcia-Orellana J, et al. Reviews and syntheses: ^{210}Pb-derived sediment and carbon accumulation rates in vegetated coastal ecosystems: setting the record straight. *Biogeosci Dis* 2018;15:1-47. DOI
15. Bos AR, Bouma TJ, de Kort GL, van Katwijk MM. Ecosystem engineering by annual intertidal seagrass beds: Sediment accretion and modification. *Estuar Coast Shelf Sci* 2007;74:344-8. DOI
16. Paquier A, Meulé S, Anthony EJ, Bernard G. Sedimentation and erosion patterns in a low shoot-density Zostera noltii meadow in the fetch-limited Berre lagoon, Mediterranean France. *J Coast Res* 2014;70:563-7. DOI
17. Gacia E, Duarte CM. Sediment retention by a mediterranean *Posidonia oceanica* meadow: the balance between deposition and

resuspension. *Estuar Coast Shelf Sci* 2001;52:505-14. DOI
18. Macreadie PI, Allen K, Kelaher BP, Ralph PJ, Skilbeck CG. Paleoreconstruction of estuarine sediments reveal human-induced weakening of coastal carbon sinks. *Glob Chang Biol* 2012;18:891-901. DOI
19. Serrano O, Lavery PS, Rozaimi M, Mateo MÁ. Influence of water depth on the carbon sequestration capacity of seagrasses. *Glob Biogeochem Cy* 2014;28:950-61. DOI
20. Miyajima T, Hori M, Hamaguchi M, et al. Geographic variability in organic carbon stock and accumulation rate in sediments of East and Southeast Asian seagrass meadows. *Glob Biogeochem Cy* 2015;29:397-415. DOI
21. Serrano O, Ricart AM, Lavery PS, et al. Key biogeochemical factors affecting soil carbon storage in Posidonia meadows. *Biogeosciences* 2016;13:4581-94. DOI
22. Villa JA, Bernal B. Carbon sequestration in wetlands, from science to practice: an overview of the biogeochemical process, measurement methods, and policy framework. *Ecol Eng* 2018;114:115-28. DOI
23. Duarte CM, Kennedy H, Marbà N, Hendriks I. Assessing the capacity of seagrass meadows for carbon burial: Current limitations and future strategies. *Ocean Coast Manag* 2013;83:32-8. DOI
24. Ward RD, Teasdale PA, Burnside NG, Joyce CB, Sepp K. Recent rates of sedimentation on irregularly flooded Boreal Baltic coastal wetlands: responses to recent changes in sea level. *Geomorphology* 2014;217:61-72. DOI
25. Alongi D, Sasekumar A, Chong V, et al. Sediment accumulation and organic material flux in a managed mangrove ecosystem: estimates of land-ocean-atmosphere exchange in peninsular Malaysia. *Mar Geol* 2004;208:383-402. DOI
26. Hyndes GA, Heck KL Jr, Vergés A, et al. Accelerating tropicalization and the transformation of temperate seagrass meadows. *Bioscience* 2016;66:938-48. DOI PubMed PMC
27. Côté-laurin M, Benbow S, Erzini K. The short-term impacts of a cyclone on seagrass communities in Southwest Madagascar. *Cont Shelf Res* 2017;138:132-41. DOI
28. Arias-Ortiz A, Serrano O, Masqué P, et al. A marine heatwave drives massive losses from the world's largest seagrass carbon stocks. *Nat Clim Chang* 2018;8:338-44. DOI
29. Macreadie PI, Anton A, Raven JA, et al. The future of blue carbon science. *Nat Commun* 2019;10:3998. DOI PubMed PMC
30. Potouroglou M, Bull JC, Krauss KW, et al. Measuring the role of seagrasses in regulating sediment surface elevation. *Sci Rep* 2017;7:11917. DOI PubMed PMC
31. Langley JA, McKee KL, Cahoon DR, Cherry JA, Megonigal JP. Elevated CO_2 stimulates marsh elevation gain, counterbalancing sea-level rise. *Proc Natl Acad Sci USA* 2009;106:6182-6. DOI PubMed PMC
32. Fourqurean JW, Duarte CM, Kennedy H, et al. Seagrass ecosystems as a globally significant carbon stock. *Nat Geosci* 2012;5:505-9. DOI
33. Robins PE, Skov MW, Lewis MJ, et al. Impact of climate change on UK estuaries: a review of past trends and potential projections. *Estuar Coast Shelf Sci* 2016;169:119-35. DOI
34. Shields E, Moore K, Parrish D. Adaptations by zostera marina dominated seagrass meadows in response to water quality and climate forcing. *Diversity* 2018;10:125. DOI
35. Leonardi N, Carnacina I, Donatelli C, et al. Dynamic interactions between coastal storms and salt marshes: a review. *Geomorphology* 2018;301:92-107. DOI
36. Waller MP, Long AJ. Holocene coastal evolution and sea-level change on the southern coast of England: a review. *J Quaternary Sci* 2003;18:351-9. DOI
37. Cundy AB, Croudace IW. Sediment accretion and recent sea-level rise in the solent, Southern England: inferences from radiometric and geochemical studies. *Estuar Coast Shelf Sci* 1996;43:449-67. DOI
38. Dyer K. The distribution and movement of sediment in the Solent, southern England. *Mar Geol* 1971;11:175-87. DOI
39. Bray MJ, Carter DJ, Hooke JM. Littoral cell definition and budgets for central Southern England. *J Coast Res* 1995;11:381-400. Available from: https://www.jstor.org/stable/4298347 [Last accessed on 28 Sep 2023]
40. SCOPAC. East Cowes to Culver Cliff; 2003, 30p. Available from: https://www.scopac.org.uk/sts/ne-iow.html [Last accessed on 28 Sep 2023].
41. New Forest District Council. SCOPAC sediment transport study, 2017. Available from: www.scopac.org.uk/sts [Last accessed on 28 Sep 2023].
42. Appleby P, Oldfield F. Application of lead-210 to sedimentation studies. In: Harmon, S editor. Uranium series disequilibrium: application to earth, marine and environmental science. 2nd ed.; Oxford: Clarendon Press; Oxford; New York: Oxford University Press; 1992. pp. 731-83. Available from: https://inis.iaea.org/search/search.aspx?orig_q=RN:25066379 [Last accessed on 28 Sep 2023].
43. Cundy A, Kortekaas S, Dewez T, et al. Coastal wetlands as recorders of earthquake subsidence in the Aegean: a case study of the 1894 Gulf of Atalantiearthquakes, central Greece. *Mar Geol* 2000;170:3-26. DOI
44. Mizugaki S, Nakamura F, Araya T. Using dendrogeomorphology and 137Cs and 210Pb radiochronology to estimate recent changes in sedimentation rates in Kushiro Mire, Northern Japan, resulting from land use change and river channelization. *Catena* 2006;68:25-40. DOI
45. Lima MAC, Ward RD, Joyce CB. Environmental drivers of sediment carbon storage in temperate seagrass meadows. *Hydrobiologia* 2020;847:1773-92. DOI
46. Amaral Camara Lima M, Ward RD, Joyce CB, Kauer K, Sepp K. Carbon stocks in southern England's intertidal seagrass meadows.

Estuar Coast Shelf Sci 2022;275:107947. DOI
47. Wentworth CK. A scale of grade and class terms for clastic sediments. *J Geol* 1922;30:377-92. DOI
48. Folk RL, Ward WC. Brazos river bar [Texas]; a study in the significance of grain size parameters. *J Sediment Res* 1957;27:3-26. DOI
49. Krishnaswamy S, Lal D, Martin J, Meybeck M. Geochronology of lake sediments. *Earth Planet Sci Lett* 1971;11:407-14. DOI
50. Appleby P, Oldfield F. The calculation of lead-210 dates assuming a constant rate of supply of unsupported 210Pb to the sediment. *Catena* 1978;5:1-8. DOI
51. Appleby P. Chronostratigraphic techniques in recent sediments. In: Tracking environmental change using lake sediments. The Netherlands: Kluwer Academic Publishers; 2001. pp 171-203. Available from: https://link.springer.com/chapter/10.1007/0-306-47669-x_9 [Last accessed on 28 Sep 2023].
52. Andersen TJ. Some practical considerations regarding the application of 210Pb and 137Cs dating to estuarine sediments. In: Weckström K, Saunders K, Gell P, Skilbeck C, editors. Applications of paleoenvironmental techniques in estuarine studies, Dordrecht: Springer; 2017, pp. 121-40. Available from: https://link.springer.com/chapter/10.1007/978-94-024-0990-1_6 [Last accessed on 28 Sep 2023].
53. Conover WJ, Iman RL. Rank transformations as a bridge between parametric and nonparametric statistics. *Am Stat* 1981;35:124-9. DOI
54. Johannessen SC. How can blue carbon burial in seagrass meadows increase the long-term, net sequestration of carbon? A critical review. *Environ Res Lett* 2022;17:093004. DOI
55. Oldfield F, Appleby PG, Battarbee RW. Alternative ^{210}Pb dating: results from the New Guinea highlands and lough Erne. *Nature* 1978;271:339-42. DOI
56. Breithaupt JL, Smoak JM, Smith TJ, Sanders CJ. Temporal variability of carbon and nutrient burial, sediment accretion, and mass accumulation over the past century in a carbonate platform mangrove forest of the Florida Everglades: carbon Burial in the coastal everglades. *J Geophys Res Biogeosci* 2014;119:2032-48. DOI
57. Shennan I. Handbook of sea-level research. In: Shennan I, Long AJ, Horton BP, editors. Handbook of Sea-Level Research. Wiley; 2015. pp. 3-25. DOI
58. Gardner L, Sharma P, Moore W. A regeneration model for the effect of bioturbation by fiddler crabs on 210Pb profiles in salt marsh sediments. *J Environ Radioact* 1987;5:25-36. DOI
59. Cearreta A, Irabien M, Ulibarri I, Yusta I, Croudace I, Cundy A. Recent salt marsh development and natural regeneration of reclaimed areas in the plentzia estuary, N. Spain. *Estuar Coast Shelf Sci* 2002;54:863-86. DOI
60. Haslett S, Cundy A, Davies C, Powell E, Croudace IW. Salt marsh sedimentation over the past c. 120 years along the west Cotentin coast of Normandy (France): relationship to sea-level rise and sediment supply. *J Coastal Res* 2003;19:609-20. Available from: https://www. jstor.org/stable/4299202 [Last accessed on 28 Sep 2023]
61. Swales A, Bentley SJ, Lovelock CE. Mangrove-forest evolution in a sediment-rich estuarine system: opportunists or agents of geomorphic change? *Earth Surf Processes Landf* 2015;40:1672-87. DOI
62. Jankowska E, Michel LN, Zaborska A, Włodarska-kowalczuk M. Sediment carbon sink in low-density temperate eelgrass meadows (Baltic Sea). *JGR Biogeosci* 2016;121:2918-34. DOI
63. Sanders CJ, Smoak JM, Sanders LM, Waters MN, Patchineelam SR, Ketterer ME. Intertidal mangrove mudflat 240+239Pu signatures, confirming a 210Pb geochronology on the southeastern coast of Brazil. *J Radioanal Nucl Chem* 2010;283:593-6. DOI
64. Macreadie PI, Ewers-Lewis JC, Whitt AA, et al. Comment on geoengineering with seagrasses: is credit due where credit is given? *Environ Res Lett* 2018;13:028001. DOI
65. Alongi D, Wattayakorn G, Pfitzner J, et al. Organic carbon accumulation and metabolic pathways in sediments of mangrove forests in southern Thailand. *Mar Geol* 2001;179:85-103. DOI
66. Greiner JT, McGlathery KJ, Gunnell J, McKee BA. Seagrass restoration enhances "blue carbon" sequestration in coastal waters. *PLoS One* 2013;8:e72469. DOI PubMed PMC
67. Duarte CM, Losada IJ, Hendriks IE, Mazarrasa I, Marbà N. The role of coastal plant communities for climate change mitigation and adaptation. *Nat Clim Chang* 2013;3:961-8. DOI
68. Baskaran M, Santschi PH. Particulate and dissolved 210Pb activities in the shelf and slope regions of the Gulf of Mexico waters. *Cont Shelf Res* 2002;22:1493-510. DOI
69. Bentley SJ, Kahlmeyer E, Bustin MR. Patterns and mechanisms of fluvial sediment flux and accumulation in two subarctic fjords: Nachvak and Saglek Fjords, Nunatsiavut, Canada. *Can J Earth Sci* 2012;49:1200-15. DOI
70. Muehlstein LK. Perspectives on the wasting disease of eelgrass Zostera marina. *Dis Aquat Org* 1988;7:211-21. Available from: http://pascal-francis.inist.fr/vibad/index.php?action=getRecordDetail&idt=19815612 [Last accessed on 28 Sep 2023].
71. Marsden A, Scott A. Inventory of eelgrass beds in Hampshire and the Isle of wight, section 2: data. Version 6. 7 May 2015. Hampshire, UK: Hampshire and Isle of Wight Wildlife Trust. Available from: https://www.researchgate.net/publication/283350752_Inventory_of_Eelgrass_Beds_in_Hampshire_and_the_Isle_of_Wight_Section_2_Data/comments [Last accessed on 28 Sep 2023].
72. Kennedy H, Beggins J, Duarte CM, et al. Seagrass sediments as a global carbon sink: isotopic constraints. *Glob Biogeochem Cy* 2010:24. DOI
73. Oreska MPI, McGlathery KJ, Emmer IM, et al. Comment on Geoengineering with seagrasses: is credit due where credit is given? 2018. Available from: https://iopscience.iop.org/article/10.1088/1748-9326/aaae72 [Last accessed on 28 Sep 2023].
74. Schile LM, Kauffman JB, Crooks S, Fourqurean JW, Glavan J, Megonigal JP. Limits on carbon sequestration in arid blue carbon

ecosystems. *Ecol Appl* 2017;27:859-74. DOI PubMed

75. Haigh I, Ozsoy O, Wadey M. et al. An improved database of coastal flooding in the United Kingdom from 1915 to 2016. *Sci Data* 2017;4:170100. DOI PubMed PMC
76. Amone-Mabuto M, Bandeira S, da Silva A. Long-term changes in seagrass coverage and potential links to climate-related factors: the case of Inhambane Bay, southern Mozambique. *WIO J Mar Sci* 2017;16:13-25. Available from: https://www.ajol.info/index.php/wiojms/article/view/159678 [Last accessed on 28 Sep 2023]
77. Preen A, Lee Long W, Coles R. Flood and cyclone related loss, and partial recovery, of more than 1000 km^2 of seagrass in Hervey Bay, Queensland, Australia. *Aquat Bot* 1995;52:3-17. DOI
78. Heck JR, Sullivan KL, Zande MJJM, Moncreiff CA. An ecological analysis of seagrass meadows of the Gulf Islands National Seashore: years one and two: seasonal assessment and inventory: interaction studies and assessment/inventory; 1995. Available from: https://cfpub.epa.gov/ols/catalog/advanced_brief_record.cfm&FIELD1=AUTHOR&INPUT1=Sullivan%20AND%20J%20AND%20S20S&TYPE1=ALL&LOGIC1=AND&COLL=&SORT_TYPE= MTIC&item_count=17&item_accn=508851 [Last accessed on 28 Sep 2023].
79. Fourqurean JW, Rutten LM. The impact of Hurricane Georges on soft-bottom, back reef communities: site- and species-specific effects in south Florida seagrass beds. *Bull Mar Sci* 2004;75:239-57. Available from: https://www.ingentaconnect.com/content/umrsmas/bullmar/2004/00000075/00000002/art00007 [Last accessed on 28 Sep 2023]
80. Anton A, Cebrian J, Duarte CM, Heck J, Kenneth L, Goff J. Low impact of Hurricane Katrina on seagrass community structure and functioning in the Northern Gulf of Mexico. *Bull Mar Sci* 2009;85:45-59. Available from: https://www.ingentaconnect.com/content/umrsmas/bullmar/2009/00000085/00000001/art00004 [Last accessed on 28 Sep 2023]
81. Pihl L, Baden S, Kautsky N, et al. Shift in fish assemblage structure due to loss of seagrass Zostera marina habitats in Sweden. *Estuar Coast Shelf Sci* 2006;67:123-32. DOI
82. Lee K, Park SR, Kim YK. Effects of irradiance, temperature, and nutrients on growth dynamics of seagrasses: a review. *J Exp Mar Biol Ecol* 2007;350:144-75. DOI
83. Collier CJ, Waycott M. Temperature extremes reduce seagrass growth and induce mortality. *Mar Pollut Bull* 2014;83:483-90. DOI PubMed
84. Egea LG, Jiménez-Ramos R, Vergara JJ, Hernández I, Brun FG. Interactive effect of temperature, acidification and ammonium enrichment on the seagrass Cymodocea nodosa. *Mar Pollut Bull* 2018;134:14-26. DOI PubMed
85. George R, Gullström M, Mangora MM, Mtolera MSP, Björk M. High midday temperature stress has stronger effects on biomass than on photosynthesis: A mesocosm experiment on four tropical seagrass species. *Ecol Evol* 2018;8:4508-17. DOI PubMed PMC
86. Hughes BB, Lummis SC, Anderson SC, Kroeker KJ. Unexpected resilience of a seagrass system exposed to global stressors. *Glob Chang Biol* 2018;24:224-34. DOI PubMed
87. Burkholz C, Duarte CM, Garcias-Bonet N. Thermal dependence of seagrass ecosystem metabolism in the Red Sea. *Mar Ecol Prog Ser* 2019;614:79-90. DOI
88. Chollett I, Bone D, Pérez D. Effects of heavy rainfall on Thalassia testudinum beds. *Aquat Bot* 2007;87:189-95. DOI
89. Campbell SJ, Mckenzie LJ. Flood related loss and recovery of intertidal seagrass meadows in southern Queensland, Australia. *Estuar Coast Shelf Sci* 2004;60:477-90. DOI
90. Nakamura Y. Patterns in fish response to seagrass bed loss at the Southern Ryukyu Islands, Japan. *Mar Biol* 2010;157:2397-406. DOI
91. Horinouchi M, Tongnunui P, Nanjyo K, Nakamura Y, Sano M, Ogawa H. Differences in fish assemblage structures between fragmented and continuous seagrass beds in Trang, Southern Thailand. *Fish Sci* 2009;75:1409-16. DOI